ACS MATERIALS Au
AN OPEN ACCESS JOURNAL OF THE AMERICAN CHEMICAL SOCIETY

pubs.acs.org/materialsau
Article

Design Principles Guiding Solvent Size Selection in ZIF-Based Type 3 Porous Liquids for Permanent Porosity

Matthew J. Hurlock, Matthew S. Christian, Jessica M. Rimsza, and Tina M. Nenoff*

Cite This: ACS Mater. Au 2024, 4, 224−237
Read Online

ABSTRACT: Porous liquids (PLs), which are solvent-based systems that contain permanent porosity due to the incorporation of a solid porous host, are of significant interest for the capture of greenhouse gases, including CO_2. Type 3 PLs formed by using metal−organic frameworks (MOFs) as the nanoporous host provide a high degree of chemical turnability for gas capture. However, pore aperture fluctuation, such as gate-opening in zeolitic imidazole framework (ZIF) MOFs, complicates the ability to keep the MOF pores available for gas adsorption. Therefore, an understanding of the solvent molecular size required to ensure exclusion from MOFs in ZIF-based Type 3 PLs is needed. Through a combined computational and experimental approach, the solvent-pore accessibility of exemplar MOF ZIF−8 was examined. Density functional theory (DFT) calculations identified that the lowest-energy solvent−ZIF interaction occurred at the pore aperture. Experimental density measurements of ZIF−8 dispersed in various-sized solvents showed that ZIF−8 adsorbed solvent molecules up to 2 Å larger than the crystallographic pore aperture. Density analysis of ZIF dispersions was further applied to a series of possible ZIF-based PLs, including ZIF−67, −69, −71(RHO), and −71(SOD), to examine the structure−property relationships governing solvent exclusion, which identified eight new ZIF-based Type 3 PL compositions. Solvent exclusion was driven by pore aperture expansion across all ZIFs, and the degree of expansion, as well as water exclusion, was influenced by ligand functionalization. Using these results, a design principle was formulated to guide the formation of future ZIF-based Type 3 PLs that ensures solvent-free pores and availability for gas adsorption.

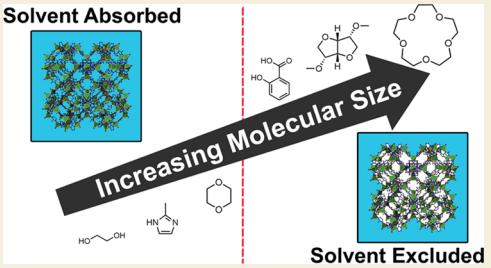

KEYWORDS: *porous liquids, metal−organic framework, MOF, zeolitic imidazole framework, solvent adsorption*

1. INTRODUCTION

Porous liquids (PLs) are an emerging material that combines the fluidity of liquids with the intrinsic porosity of solids sorbents.[1−6] PLs are categorized into four classes or types. Type 1 PLs are neat liquids composed of discrete partials that contain pore space, such as surface-functionalized hollow silica nanospheres.[7−9] Type 2 PLs are formed from dissolved nanoporous macromolecules, such as porous organic cages or metal−organic polyhedra, in a sterically bulky solvent that is too large to occupy the pores.[10−12] Type 3 PLs are dispersions of solid porous materials, such as metal−organic frameworks (MOFs) or zeolites, in bulky solvents.[13−16] The final type, Type 4, is neat liquids formed from extended frameworks that maintain porosity in a liquified state.[17]

Type 3 PLs are a promising tunable platform for the development of gas capture materials that builds upon research into solid sorbent materials.[18] Among solid sorbents used for Type 3 PLs, MOFs offer a unique opportunity to study the structure−property relationship between adsorption and porosity due to the ease of tunability of the porous frameworks.[19−21] For example, MOFs can be judicially designed to tune the desired properties such as pore size, ligand functionality, and metal center.[22,23] Additionally, the surface of MOFs can be readily functionalized, allowing improved dispersion within liquids.[24−26] ZIF−8 is a MOF from the zeolitic imidazole framework (ZIF) family that has recently shown promise for use in Type 3 PLs.[27−30] This is due to the high hydrophobicity of the framework, which excludes water from the pores except under high hydrostatic pressures.[31] As a result, ZIF−8 and related surface-functionalized versions have been shown to improve the uptake of gases, including CO_2 and O_2, in both water and water−organic solvent mixtures.[6,31−33] However, aqueous ZIF-based PLs are not without other challenges. The formation of carbonates from the reaction of CO_2 with the solvent system can lead to framework degradation over time.[34]

Though ZIF-based PLs show promise as gas capture materials, there is little understanding for these systems of what constitutes a sterically bulky solvent and what solvent−sorbent interactions occur. Solid ZIF−8 can adsorb gas molecules with kinetic diameters more than double the size

Received: November 1, 2023
Revised: December 15, 2023
Accepted: December 18, 2023
Published: December 29, 2023

https://doi.org/10.1021/acsmaterialsau.3c00094
ACS Mater. Au 2024, 4, 224−237

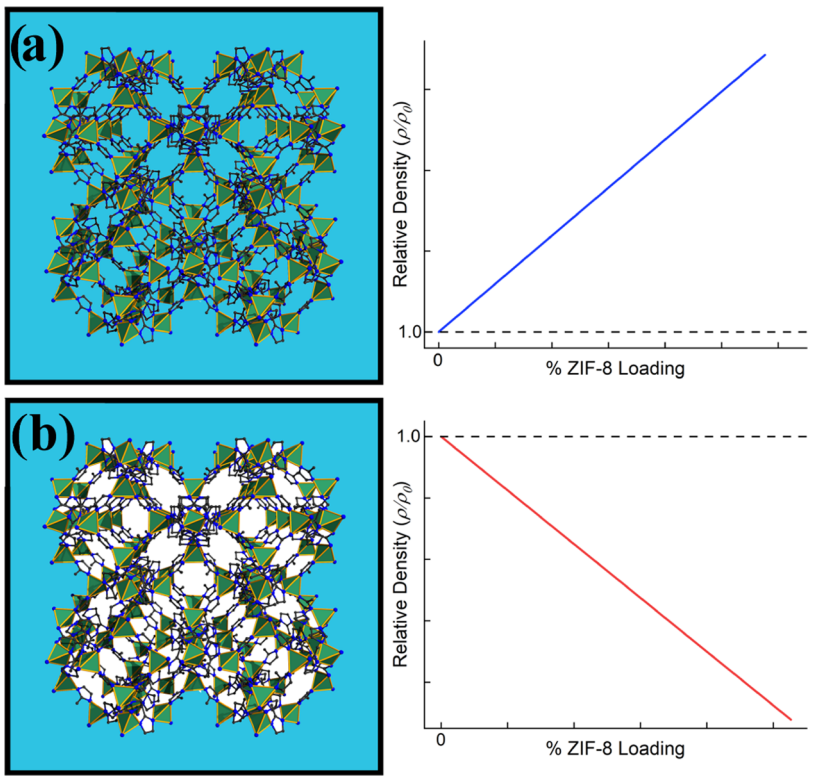

Figure 1. Illustration of the density trend with increased ZIF loading of a ZIF−8 dispersion when (a) the solvent is small and adsorbed into the pores or (b) the solvent is too sterically bulky and excluded from the pores. (Atom colors: zinc green polyhedrons, carbon black spheres, nitrogen blue spheres, and hydrogen omitted for clarity).

of the crystallographic pore aperture of the framework, further complicating solvent adsorption predictions.[35] This phenomenon is known as gate-opening and is defined as the expansion of the pore aperture caused by rotation of the 2-methylimidazole ligands at that site upon interaction with guest molecules.[36−39]

Recently, it has been shown that density measurements can be used to probe the pore availability, i.e., whether the pores are occupied or unoccupied by solvent molecules.[31] In general, the density of a PL is measured at varying loadings of sorbent. As depicted in Figure 1, the results can then be compared to two sets of theoretically calculated densities, one where the pores are assumed filled with the bulk solvent and the other where it is assumed the pores are empty. From this comparison, it can be determined whether a solvent is adsorbed into the pores, Figure 1a, or excluded, Figure 1b. To date, most Type 3 PL systems have not been analyzed with this method.

Computational modeling approaches can further help us understand gate-opening mechanisms. Methods such as density functional theory (DFT), can be used to calculate the binding energies for gases and solvent molecules inside ZIFs, the energy barrier for molecules to move between ZIF pores, and the deformation of the pore aperture as a molecule approach.[40−42] However, previous investigations of energetic barriers and gate-opening, using either classical approaches in periodic crystalline ZIFs[43,44] or through simple molecular representations of the ZIF pore aperture using first principal approaches,[45−48] have not examined the gate-opening phenomenon of a ZIF cluster.

Herein, we systematically analyze the availability of the porosity of ZIFs dispersed in various solvents using computation calculations and density measurements. First, calculations of solvent−ZIF−8 interactions suggest favorable interactions at the pore aperture and that solvents previously used in ZIF−8 PLs are adsorbed by the framework. From the density analysis of single-component solvent systems, the exclusion size of solvent molecules for ZIF−8 was determined. Next, the preferential adsorption of solvents within mixed solvent systems was further examined using thermogravimetric mass spectroscopy analysis of ZIF−8 dispersions in a ternary mixture of water, ethylene glycol, and 2-methylimidazole. This density analysis methodology was further applied to a series of ZIFs with varying structures, including ZIF−67, −69, −71-(RHO), and −71(SOD), to examine the effects of metal node identity, pore size, framework topology, and ligand functionality on the exclusion of solvents from the framework. Finally, a design principle is proposed to guide the design of future ZIF-based Type 3 PLs ensuring pore availability for gas adsorption.

2. EXPERIMENTAL SECTION

2.1. Computational Methods

A ZIF−8 particle was created from a ZIF−8 crystal structure, shown in Figure S1a, and placed in a 37 Å^3 periodic box.[49] The cleavage of the particle from the crystalline structure creates two unique pore apertures, illustrated in Figure S1b,c. A potential energy surface (PES) was sampled for CO_2, ethylene glycol (EG), and water for both pore apertures in 0.1 Å increments by moving the solvent molecules of interest from the edge of the periodic cell through the pore aperture and into the ZIF−8 pore, creating 50 different sampling points. 2-methylimidazole (HMIm) was also analyzed but only for the larger pore opening due to the molecule possessing a significantly larger size than the pore aperture diameter. The coordinates for the central atom of each solvent molecule were frozen to keep the molecule from migrating from the PES pathway.

https://doi.org/10.1021/acsmaterialsau.3c00094
ACS Mater. Au 2024, 4, 224−237

Density functional theory (DFT) calculations were carried out using the Fritz Haber Institute Ab-Initio Molecular Simulations (FHI-AIMS) package for efficient computation of DFT energies and forces.[50−53] All DFT calculations used the PBE exchange-correlational functional with 0.1 eV Gaussian smearing. van der Waals dispersion interactions were included using the Tckenko−Sheffler (vdw-TS) method[54] and included relativistic effects via atomic scalar ZORA corrections.[51] SCF energy and /Å^3 and each calculation used a single γ-point k-point mesh. The adsorption energy of the molecule to ZIF−8 was calculated via eq 1, which is the difference between the energy of the ZIF−8 + molecule and the individual molecule and ZIF−8 particle.

$$E_{Ads} = E_{ZIF\text{-}8+molecule} - E_{ZIF\text{-}8} - E_{molecule} \quad (1)$$

2.2. Materials

Zinc nitrate hexahydrate (98%), cobalt nitrate hexahydrate (99%), 2-methylimidazole (99%; HMIm), 1-methylimidazole (99%; 1MIm), 2-nitroimidazole (98%), 4,5-dichloroimidazole, 5-chlorobenzimidazole (96%), 2′-hydroxyacetophenone (99%; 2HAP), 2-chlorophenol (99%; 2CP), Cyrene (dihydrolevoglucosenone, DHLC), dimethyl isosorbide (99%; DMI), p-dioxane (p-diox), 1-propanol, N,N-dimethylformamide (99.8%; DMF), 15-crown-5 (98%, 15C5), and ethylene glycol (99.8%; EG) were purchased from Sigma-Aldrich. Methanol was purchased from CMC Materials, and zinc acetate hexahydrate (98%) was purchased from Acros Organics. He (99.999%) and N_2 (99.999%) gases were purchased from Matheson Trigas. All chemicals were used as received.

2.3. Synthesis of ZIF Materials

ZIF−8 was synthesized through modification of a previously reported method.[55] Separately, both 2-methylimidazole (13.0 g, 158 mmol) and zinc nitrate hexahydrate (5.8 g, 19 mmol) were each dissolved in 200 mL of methanol. Next, the zinc nitrate solution was added to the 2-methylimidazole solution while the mixture was stirred at 850 rpm. The mixture was stirred for 1 h at room temperature, resulting in an opaque white solution. The ZIF−8 solid was removed from solution by centrifugation at 9500 rpm for 10 min. The solid was then washed three times with methanol and soaked in fresh methanol for 24 h. After the solid was removed from solution one last time, the solid was dried in an oven at 60 °C for 6 h, yielding 1.36 g of ZIF−8.

ZIF−67 was synthesized following a previously reported method.[31] Separately, both 2-methylimidazole (3.24 g, 39 mmol) and cobalt nitrate hexahydrate (1.44 g, 8 mmol) were each dissolved in 200 mL of methanol. Next, the cobalt nitrate solution was added to the 2-methylimidazole solution with stirring at 850 rpm. Stirring was continued for 12 min at room temperature, resulting in an opaque purple solution. The solution was then kept undisturbed for 24 h at room temperature. After this time, the purple solid ZIF−67 was removed from solution by centrifugation at 9500 rpm for 20 min. The solid was then washed three times with methanol and soaked in fresh methanol for 24 h. After the solid was removed from solution one last time, the solid was dried in an oven at 60 °C for 6 h, yielding 0.374 g of ZIF−67.

ZIF−69 was synthesized following a previously reported method.[55] Solutions of 2-nitroimidazole (0.362 g, 3 mmol) in 16 mL of DMF, 5-chlorobenzimidazole (0.488 g, 3 mmol) in 16 mL of DMF, and zinc nitrate hexahydrate (0.476 g, 16 mmol) in 8 mL of DMF were combined in a 45 mL Teflon lined Parr reactor. The reactor was sealed and heated at 95 °C for 3 days. After cooling the orange solid ZIF−69 was collected with centrifugation at 4000 rpm for 5 min and washed three times with DMF. The solid was then soaked in fresh DMF for 24 h. After this, the solid was centrifuged and washed three times with methanol and then soaked for 24 h in fresh methanol. After the solid was removed from the solvent one last time, it was dried in an oven at 60 °C for 6 h, yielding 0.409 g of ZIF−69.

ZIF−71(RHO) was synthesized following a previously reported method.[55] Separately, 4,5-dichloroimidazole (0.876 g, 6 mmol) and zinc acetate hexahydrate (0.297 g, 1 mmol) were each dissolved in 60 mL of methanol. Next, the zinc acetate solution was added to the 4,5-dicholoroimidazole solution, and the mixture was briefly shaken to mix the two solutions. The mixture was kept undisturbed at room temperature for 24 h. After this time the pink-white solid ZIF−71(RHO) was removed from solution by centrifugation at 4000 rpm for 5 min. The solid was then washed and centrifuged three times with methanol and soaked in fresh methanol for 24 h. After the solid was removed from the solvent one last time, the solid was dried in an oven at 60 °C for 6 h, yielding 0.432 g of ZIF−71(RHO).

ZIF−71(SOD) was synthesized following a previously reported method.[55] First, 1-methylimidazole (0.88 g, 11 mmol) was added to a solution of 4,5-dichloroimidazole (1.466 g, 011 mmol) in 100 mL of 1-propanol. Next, zinc nitrate hexahydrate (0.796 g, 3 mmol) was dissolved in 100 mL of 1-propanol. The 4,5-dichloroimidazole solution was added to the zinc nitrate solution while stirring. The resulting transparent yellow-brown solution was stirred at 850 rpm for 48 h. Then, the off-white solid ZIF−71(SOD) was removed from solution by centrifugation at 4000 rpm for 5 min. The solid was then washed three times with methanol and soaked in fresh methanol for 24 h. After the solid was removed from solution one last time, the solid was dried in an oven at 60 °C for 6 h, yielding 0.688 g of ZIF−71(SOD).

2.4. Instrumentation

Density measurements were performed using a Micromeritics AccuPyc 1300 He pycnometer with a 1 cm^3 cell insert. X-ray diffraction (PXRD) measurements were obtained using a Bruker D2 Phaser with a LYNXEYE XE-T detector and 30 kV Cu Kα1 radiation (λ = 1.5406 Å) at room temperature. XRD of PLs was performed on 500 μL aliquot samples of 10 wt % PLs after vigorously mixing the PL using a vortex stirrer. Fourier transform infrared (FTIR) spectra were collected on a Thermo Fisher Nicolet IS10 instrument with a SMART iTR attenuated total reflectance (ATR) attachment. Nitrogen gas adsorption isotherms were obtained using a Micromeritics ASAP 2020. All ZIF samples were activated at 150 °C for 5 h before analysis. Thermogravimetric analysis coupled mass spectrometry (TGA-MS) was performed on a TA Instruments Discovery SDT 650. Samples were heated from room temperature to 30 °C and held isothermally for 30 min. Then, the temperature was increased to 1000 °C at a ramp rate of 1 °C/min under a He flow of 100 mL/min.

2.5. Methods

2.5.1. Porous Liquid Formation. Porous liquids were made through modification of our previously reported methods.[34] In general, to make a uniform colloidal dispersion, ZIF was added to the solvent, followed by vortex stirring and sonication. For example, a 10 wt % (wt %) ZIF−8 PL in water was made by adding 0.300 g of dried ZIF−8 to 2.700 g of H_2O. The solution was then vortexed for 30 s followed by sonication for 10 min. ZIFs were recovered post measurement from the various solvent dispersions through centrifugation at 9500 rpm and washing with methanol. After being soaked in fresh methanol for 24 h, the recovered ZIFs were dried at 60 °C for 6 h.

2.5.2. Density Measurements. Through modification of previously reported methods,[30,31,56] the densities of ZIF samples were measured while dispersed in various solvents at concentrations between 0 and 20 wt % ZIF. Lower-loading ZIF dispersions were made through serial dilution of the higher-concentration dispersions. Selected properties of examined solvents, including vapor pressure, and comparison of each solvent density with its measured densities are compiled in Table S1. For solvents with vapor pressures below water (P < 3.17 kPa; 2CP, 2HAP, 1MIm, DMI, EG, 15C5, and DHLC) the density of the dispersions was determined by He pycnometry. Specifically, the aluminum cup insert was washed with acetone and then held in an oven at 110 °C for 30 min. The dried cup was removed from the oven and cooled to room temperature in a desiccator. The mass of the cup was measured five times and the average was used for density calculations. Next, approximately 1 mL of ZIF dispersion was added to the cup and the average combined mass over five measurements was used for density measurements. The mass difference of the empty and filled cup was calculated and represents the mass of the ZIF dispersion. Then, the cup containing

https://doi.org/10.1021/acsmaterialsau.3c00094
ACS Mater. Au 2024, 4, 224−237

the ZIF dispersion was placed in the He pycnometer and the volume of the slurry was averaged from ten measurements. Finally, the density of the dispersion was determined, by dividing the mass of the ZIF dispersion, by each volume and averaging the results.

For solvents with vapor pressures at or above water ($P \geq 3.17$ kPa; water and *p*-diox), the density of the solutions was determined using a 2 mL glass pycnometer. Specifically, the glass pycnometer was washed with acetone and then kept in an oven at 110 °C. The dried glass pycnometer was removed from the oven and cooled to room temperature in a desiccator. Then the mass of the empty pycnometer was measured five times, and the average mass was used for the density calculations. Next, the solution was added to the glass pycnometer until full, and the cap was placed on top. Any excess solvent that was pushed out of the pycnometer was wiped off. The average mass of the filled pycnometer over five measurements was used for density calculations. The density of the PL was determined by dividing the mass of the PL, determined by subtracting the mass of the empty pycnometer from the filled pycnometer by the volume of the pycnometer, 2.00 mL.

Partial molar volume: Partial molar volumes of formed PLs were calculated following previously reported methods.[56] In general, the measured density (g/mL) of the formed dispersions was plotted as a function of the ZIF concentration (g/mL). The data was fitted linearly with a fixed slope, and the slope and y-intercept of the fitted line were used to calculate the partial molar volume of the ZIFs. Molar volumes of ZIFs were determined using reported crystallographic data.[55,57,58]

3. RESULTS AND DISCUSSION

3.1. Computational Analysis of Guest−ZIF−8 Interactions

Mixed solvent systems, composed of two or more solvent components, are of particular interest by providing another mechanism of tuning the properties of the PLs.[6] Previous DFT computational studies of CO_2 interactions with the components of the solvent systems studied here (water/ethylene glycol/2-methylimidazole) indicate that the CO_2 molecule is overall stable and is not expected to be form additional chemical species in the PL.[34] In this study, DFT calculations using a solvated ZIF−8 particle were performed to elucidate the solvent−ZIF interactions that influence the adsorption of solvent molecules. Using a known ZIF−8 PL capable of capturing carbon dioxide as the exemplar system,[6] potential energy surfaces (PES) were calculated from the adsorption energies for each of the solvent molecules in the three component solvent system: water, EG, and HMIm as well as CO_2. These calculations were performed for both the large and small pore apertures of the ZIF−8 particle, determined to be 5.0 and 2.4 Å, respectively, measured as the H···H distance of HMIm ligands across the apertures, Figure S1. The results for PES are shown in Figure 2 for both pore apertures.

All molecules possessed similar behaviors as each approached the pore apertures of ZIF−8. For the larger pore aperture (5.0 Å), the adsorption energies for the solvent molecules began to steeply decrease approximately 1.5 Å from the aperture, as shown in Figure 2a, due to interactions between the solvent molecules and the HMIm ligands on the ZIF−8 surface. Maximum adsorption energies between the molecules and the large pore aperture occurred when the molecule was 0.5−0.2 Å away from the aperture. Meanwhile, maximum adsorption energies for the smaller aperture occurred when the solvent molecules were between 1.0 and 0.5 Å away from the pore aperture, Figure 2b. The molecular adsorption energies (global minimum) are similar for both pore apertures and are proportional to the size of the adsorbed molecule (HMIm > EG > CO_2 ~ H_2O). Adsorption energy

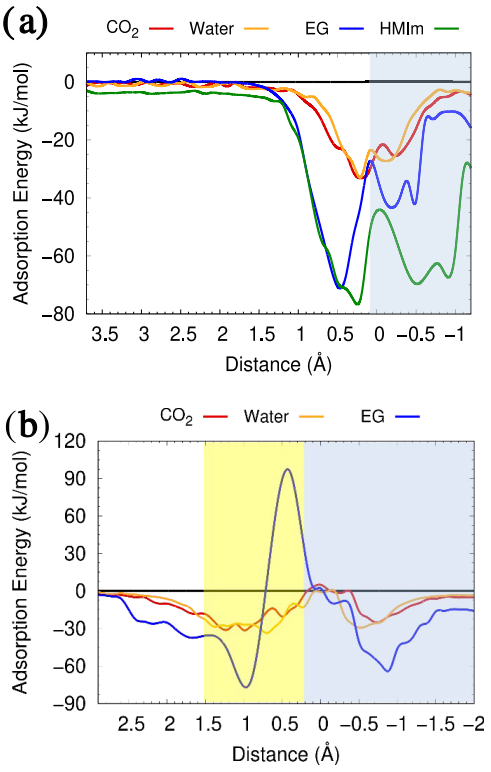

Figure 2. PES of the solvent molecules water (orange line), EG (blue line), HMIm (green line), and CO_2 gas (red line) moving through (a) the large 5.0 Å pore aperture and (b) the smaller 2.4 Å pore aperture as a function of distance from the pore. The yellow section indicates the region where the molecules are within the pore aperture of ZIF−8, and the blue region indicates where the molecules are inside the pore space.

then increased as the molecules reached a thermodynamic barrier, a local maximum for the larger pore aperture, Figure 2a, and a global maximum for the smaller pore aperture, Figure 2b.

The PES curves indicate that there is only a small (~7 kJ/mol) energy barrier for both water and CO_2 to enter the pore through the smaller pore aperture, as shown in Figure 2b. However, the large increase in the adsorption energy for EG at 0.5 Å in Figure 2b indicated that the aperture is too small for EG to pass through and enter the pore space. Compared to the small pore, all four molecules passed through the larger pore aperture without an energy barrier. During infiltration expansion of both pore apertures, also known as gate-opening,[36−39] occurred. The small pore aperture expanded from 2.4 to 4.2 Å upon adsorption of CO_2, Figure S2, while large pore aperture expanded from 5.0 to 6.2 Å upon adsorption of HMIm, illustrated in Figure S3. Additionally, the energy barrier for pore entry was a local maximum in the PES curves and indicated that adsorption of solvents is kinetically driven for molecules to enter the pore.

Figures S4 and S5 decompose the molecular PES into van der Waals and electrostatic contributions. All systems, with the exception of water, have the strongest van der Waals interactions near the pore aperture and increase sharply when passing through the pore aperture. In comparison, the electrostatic contribution has the greatest interaction in the pore opening, leading to the lowest energy point in the overall PES and indicating that electrostatic repulsion increases as the molecules approach the aperture.

https://doi.org/10.1021/acsmaterialsau.3c00094
ACS Mater. Au 2024, 4, 224−237

Together, this demonstrates that both solvent and gas molecules interact strongly at the pore aperture and may lead to competitive adsorption within ZIF-based PL systems at these sites.

3.2. Formation and Characterization of ZIF-Based PLs

To evaluate ZIF−8 infiltration by organic solvents, dispersions of ZIF−8 were made over a range of ZIF loadings (0−20 wt %) and using multiple organic solvents of varying molecular sizes including EG, 1MIm, *p*-diox, 2CP, 2HAP, and DHLC. Note, gelation occurred in dispersions with ZIF−8 loading higher than 20 wt %. To ensure an even suspension, the dispersions were vigorously stirred and sonicated. Resulting ZIF−8 dispersions were characterized with XRD and FTIR to examine the stability of the systems and are provided in the Supporting Information Figures S9 and S10. FTIR spectra demonstrated that no change in the chemical bonding of ZIF−8 or the solvents occurred upon formation of the dispersions, and all spectra were a combination of bulk ZIF−8 and solvent. XRD was used for the formed dispersions and post dispersion, to ensure that no framework degradation had occurred when ZIFs were mixed with solvents. The XRD diffraction patterns of the formed ZIF-liquid dispersions generally consisted of some characteristic reflections of the ZIF along with an increased amorphous contribution from the solvent at higher degrees 2θ. Together, the results of both characterization techniques illustrated that all of the ZIF-solvent dispersion combinations were stable.

Though XRD confirmed the framework stability after dispersion formation, there were changes in the relative reflection intensities between bulk solid ZIF−8 and the ZIF−8 dispersions formed. For example, as shown in Figure 3a, the (110) reflection at 7.4° 2θ is the highest-intensity reflection in bulk ZIF−8. This is in contrast with ZIF−8 dispersed in EG where the (112) and (222) reflections at 12.4 and 18.1° 2θ, respectively, became the highest-intensity reflections and the (110) reflection was among the lowest. This decrease in reflection intensity at low 2θ suggests the presence of guest molecules in the pores of the MOF.[59,60] However, ZIF−8 dispersions formed using sterically bulky solvents that are excluded from the pores, such as 2HAP discussed in Section 3.5, also showed similar intensity shifts in Figure 3a. This suggests that an interaction at the solvent−ZIF interface resulted in reflection intensity shifts, which has been known to occur in other MOF-based PLs with solvents of varying sizes.[14] A similar intensity ratio of the bulk solid is regained upon separation, washing, and drying of ZIF−8 from the solvents; see Figure 3b, further indicating ZIF−8 stability within the solvents. Similar changes in reflection intensity upon dispersion formation also occurred for other ZIF (ZIF−67, −69, and −71) dispersions, Figures S11−S18.

3.3. Effects of Solvent Mixing on Solvent Exclusion ZIF−8 PLs

Recent work has shown that density analysis can be used as a simple method to evaluate the availability of host porosity within PL systems.[31,56] The density of ZIF−8 (0.943 g/mL), which was determined using crystallographic data following previously reported methods,[31,56] is smaller than the densities of the many typical solvents. Therefore, the relative density of a ZIF−8 PL is expected to decrease with increasing ZIF loading as the solvent molecules are too large to be adsorbed.

Density analysis was used to determine the availability of ZIF−8 porosity in an exemplary solvent mixture composed of water, EG, and HMIm in a ratio of 40:35:25 by mass. For comparison single-component density studies were first performed, see Figure 4. The results indicated that EG is adsorbed by ZIF−8 since the measured densities increase with increasing ZIF−8 loading. However, the decreasing densities at increased ZIF−8 loading indicated that water was excluded from the pores due to framework hydrophobicity, which is further discussed in Section 3.5. The compound HMIm was anticipated to be adsorbed into the pores of ZIF−8 as it is similar in size to 1MIm, discussed in Section 3.5. This was confirmed using a binary solvent mixture of 25 wt % HMIm in water (Figure 4), where the densities of the system increased with increased ZIF−8 loading. These results validate the favorable adsorption of EG and HMIm observed computationally.

As predicted by the single and binary systems, the density of the ternary mixture of water, EG, and HMIm also possessed an increased density at higher loadings of ZIF−8, Figure 4, due to solvent adsorption. To determine if there was preferential

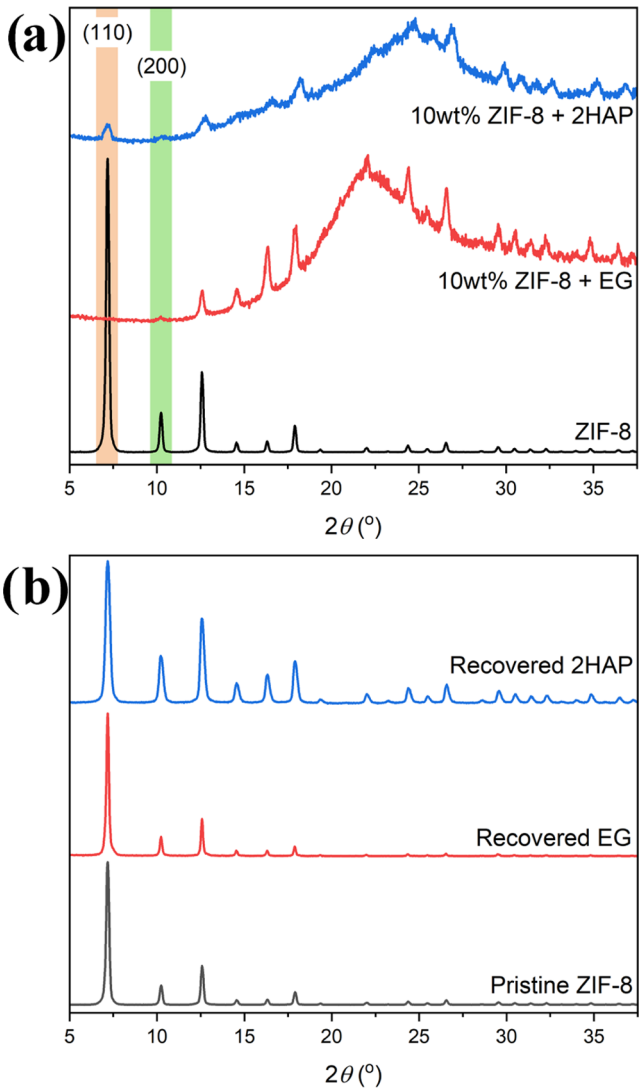

Figure 3. XRD patterns comparing (a) bulk ZIF−8 (black) to a 10 wt % ZIF−8 dispersion in EG (red) and 2HAP (blue) with the (110) and (200) reflections highlighted orange and green, respectively, and (b) pristine ZIF−8 (black) to ZIF−8 recovered from a 10 wt % ZIF−8 dispersion in EG (red) and a 10 wt % ZIF−8 dispersion 2HAP (blue).

https://doi.org/10.1021/acsmaterialsau.3c00094
ACS Mater. Au 2024, 4, 224−237

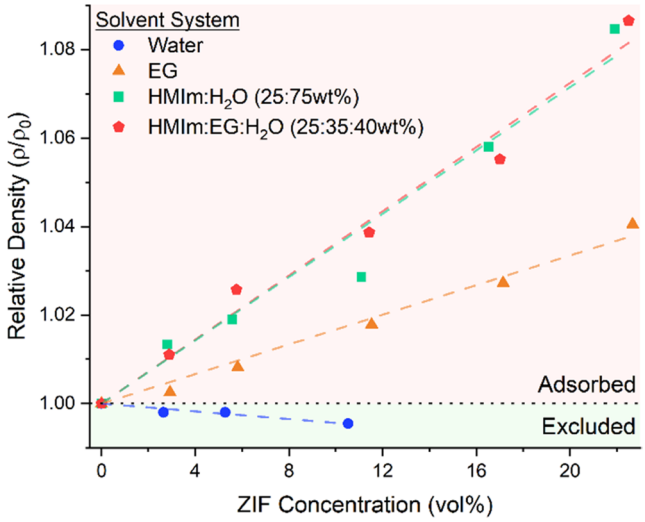

Figure 4. Relative measured densities of dispersions containing various loadings of ZIF−8 in water (blue circles), EG (orange triangles), a mixture of 25 wt % HMIm in water (green squares), and a mixture of HMIm, EG, and water at 25:35:40 wt % respectively (red pentagons).

adsorption between EG or HMIm, TGA-MS was performed on a 10 wt % ZIF−8 dispersion in the ternary solvent mixture. The data show a large mass loss from 30 to 175 °C due to the loss of bulk solvents from the ZIF dispersion, Figure S19. When compared to bulk ZIF−8 and the bulk ternary mixture, the TGA plot of the 10 wt % ZIF−8 dispersion showed an additional mass loss step at 250 °C due to the loss of adsorbed solvents within the pores of ZIF−8. Increases in the ion current occurred for both water and HMIm, but not EG, indicating that HMIm is preferentially adsorbed over EG. Furthermore, it suggests that mixed solvent systems allow for the adsorption of solvents that were excluded from the ZIF−8 pore in single-component dispersion experiments. This is likely due to pore aperture expansion caused by the other solvent molecules present.

3.4. Structural Influences on Water Exclusion in ZIF-Based PLs

The structural factors that influence water exclusion from the porous hosts are important in the design of PLs. Due to its molecular size, water is difficult to exclude from the pores of many MOFs through steric factors alone. The wide structural variety within the ZIF MOF family allows for the examination of structure−property relationships within related Type 3 PL systems. Water exclusion was examined using ZIFs ZIF−8, −67, −69, and −71. ZIF−71 possess two unique topologies (**rho** and **sod**) that can be formed from the same ligand−metal combination (Zn^{2+} and 4,5-dichloroimidazole) through control of synthetic conditions.[55,61,62] Both structures were examined in this work and are identified as ZIF−71(RHO) and ZIF−71(SOD), for the **rho** and **sod** topologies, respectively. A comparison of the structures and properties of these ZIFs is provided in the Supporting Information, pages S5−S7.

Density measurements of the five ZIFs dispersed in water were collected and are shown in Figure S20 and compared in Table 1. ZIF−8 was used as the exemplar MOF since water does not enter the pores due to framework hydrophobicity.[35,63] Water exclusion from the pores was confirmed as the measured densities of the ZIF−8-water PL align well with theoretical densities of the system when the pores of the framework are empty. Through comparison with calculated theoretical densities, water was determined to be excluded from the pores of ZIF−67 as well as the large pored ZIF−71(RHO) and −71(SOD) but was adsorbed by ZIF−69 (see Table 1). This is further illustrated by the change in the partial molar volumes of ZIF−69, shown in Figure S21, which decreased almost 40% while the partial molar volumes of ZIF−8, −67, and −71(SOD) showed little deviation. This decrease indicated that the molar volume added by ZIF−69 is less than the molar volume of the bulk solid due to water adsorption. In contrast, the partial molar volume of ZIF−71(RHO) dispersed in water showed a dramatic increase of 71% and a decrease in densities below the theoretical calculated densities was observed. This is likely caused by interparticle void space formation due to aggregation of the highly hydrophobic ZIF−71(RHO) particles, which caused an increase in the ZIF−71(RHO) dispersion volume and deviation in the measured densities from theoretically calculated densities.

Table 1. Densities of ZIF−Water Dispersions at 10 wt % ZIF Compared to the Theoretical Density of a 10 wt % ZIF−Water Dispersion When Water Is Assumed Adsorbed or Exclude from the Pores

ZIF	theoretical density adsorbed (g/mL)	measured density (g/mL)	theoretical density excluded (g/mL)
ZIF−8	1.042	0.987	0.986
ZIF−67	1.037	0.979	0.988
ZIF−69	1.036	1.032	0.992
ZIF−71(RHO)	1.040	0.931	1.006
ZIF−71(SOD)	1.080	1.023	1.022

However, it is known that ZIF−71(RHO) adsorbs water vapor and that the density of water does decrease when confined in nanoporous materials.[64−66] TGA-MS analysis indicated in Figure S22 that there is no additional adsorbed solvent mass loss in the TGA or a substantial difference in the MS signal of water for the 10 wt % ZIF−71(RHO)−water dispersion compared to the bulk ZIF−71(RHO). This demonstrated that the density measurements were correct and water was not adsorbed by ZIF−71(RHO) when dispersed in water. Overall, the observed trend of water exclusion from the pores of the ZIFs aligns with the hydrophobicity of the frameworks,[55] where the polar functionalities on the ligands of ZIF−69 decrease the hydrophobicity of the framework compared to the other ZIFs, allowing water to be adsorbed into the pores.

3.5. Pore Aperture Expansion Effects on Solvent Exclusion in ZIF−8 PLs

Pore aperture expansion of ZIF−8 complicates the predictability of solvent exclusion based on crystallographic data. Density measurements were further used to assess the effects of pore aperture expansion on the solvent accessibility of the porosity within ZIF−8 Type 3 PL systems. ZIF−8 dispersions were made using varying sizes of solvent molecules to determine the limit of adsorbed molecule size in ZIF−8. The van der Waal volumes (V_W) of the solvent molecules were calculated using reported methods,[67] and were used to approximate the molecular diameters (d_W) of the solvents. The d_W of the evaluated solvents ranged from 3.2 to 7.4 Å/molecule. The V_W and d_W of the chosen solvents, along with

https://doi.org/10.1021/acsmaterialsau.3c00094
ACS Mater. Au 2024, 4, 224−237

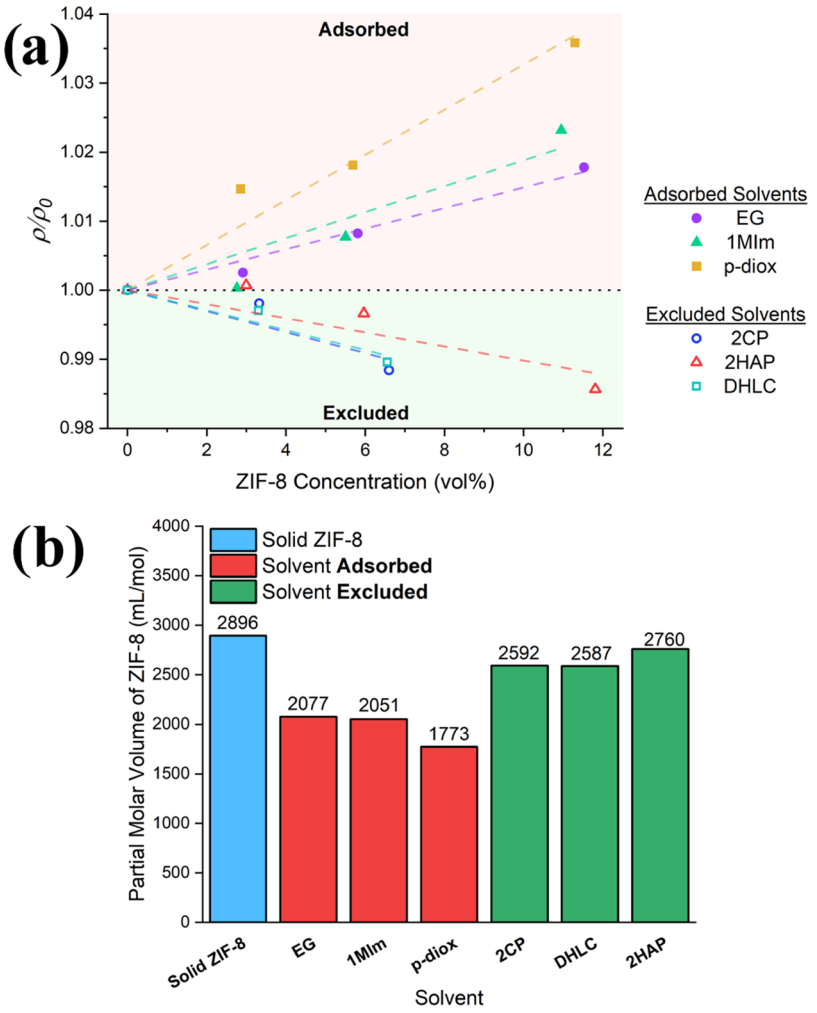

Figure 5. (a) Relative measured densities of dispersions containing various loadings of ZIF−8 in water (blue circles), EG (orange triangles), 1MIm (green squares), *p*-dioxane (red diamonds), 2CP (gold pentagons), and 2HAP (purple hexagons). (b) Comparison of the molar volume of ZIF−8 (blue) with the partial molar volumes of ZIF−8 dispersions in adsorbed solvents (red) and exclude solvents (green).

other selected properties, are summarized in Tables S3−S5. Results showed that calculated d_W compared well with previously reported kinetic diameters,[35] illustrating ease and consistency in this method to estimate molecular size. Additionally, the measured densities of the neat solvents showed little deviation from manufacturer-supplied values, Table S3, further supporting the accuracy of this measurement methodology.

Again, due to the lower density of ZIF−8 (0.943 g/mL) compared to the densities of the examined solvents, the density of ZIF−8 solvent dispersions is expected to decrease with increasing ZIF loading when a PL is formed as the solvent molecules are too large to be adsorbed. Figure 5a shows the comparison relative densities of ZIF−8 dispersed in the individual solvents EG, 1MIm, *p*-diox, 2CP, DHLC, and 2HAP. The densities of the dispersions formed by using the solvents EG, 1MIm, and *p*-diox increased with increasing ZIF−8 loading. By contrast, the dispersions made using 2CP, DHLC, and 2HAP solvents decreased in densities with increasing ZIF−8 loading. This indicates that solvent molecules with $d_W \leq 5.4$ Å/molecule are adsorbed by the MOF and occupy the pores, while molecules with $d_W > 5.4$ Å/molecule are too large to be adsorbed and are excluded from the pores of ZIF−8, forming a PL.

This solvent molecule size cutoff of 5.4 Å/molecule is larger than the ZIF−8 crystallographic pore aperture of 3.4 Å.[58] Which indicates that expansion of the ZIF−8 pore aperture occurred, allowing adsorption of molecules larger than the crystallographic pore aperture. Furthermore, the experimental expansion of the pore aperture to between 5.4 and 5.9 Å aligns well with computational results.

Previous investigations have shown that expansion of the pore aperture of ZIF−8 allowed for the adsorption of gases with kinetic diameters of up to 7.6 Å.[35] However, our size exclusion limit for solvent molecules adsorbed into the pores of ZIF−8 is smaller than that for adsorbed gas vapors. This difference is likely due to temperature effects, as the gas vapor adsorption studies were performed at elevated temperatures.

From density measurements of the PLs, the partial molar volumes of ZIF−8 were calculated, Figure 5b, and are useful as a simple comparison method.[56] The results showed that the volume contribution of ZIF−8 in solvents possessing a d_W greater than 5.4 Å is similar to that of bulk ZIF−8 and decreased less than 15%, Figure S23. This further confirms that these solvents are excluded from the pores of the framework, as the volume contribution of ZIF−8 is unchanged in the PLs compared to the bulk solid. By contrast, dispersions formed from solvents smaller than 5.4 Å showed a decrease in the

https://doi.org/10.1021/acsmaterialsau.3c00094
ACS Mater. Au 2024, 4, 224−237

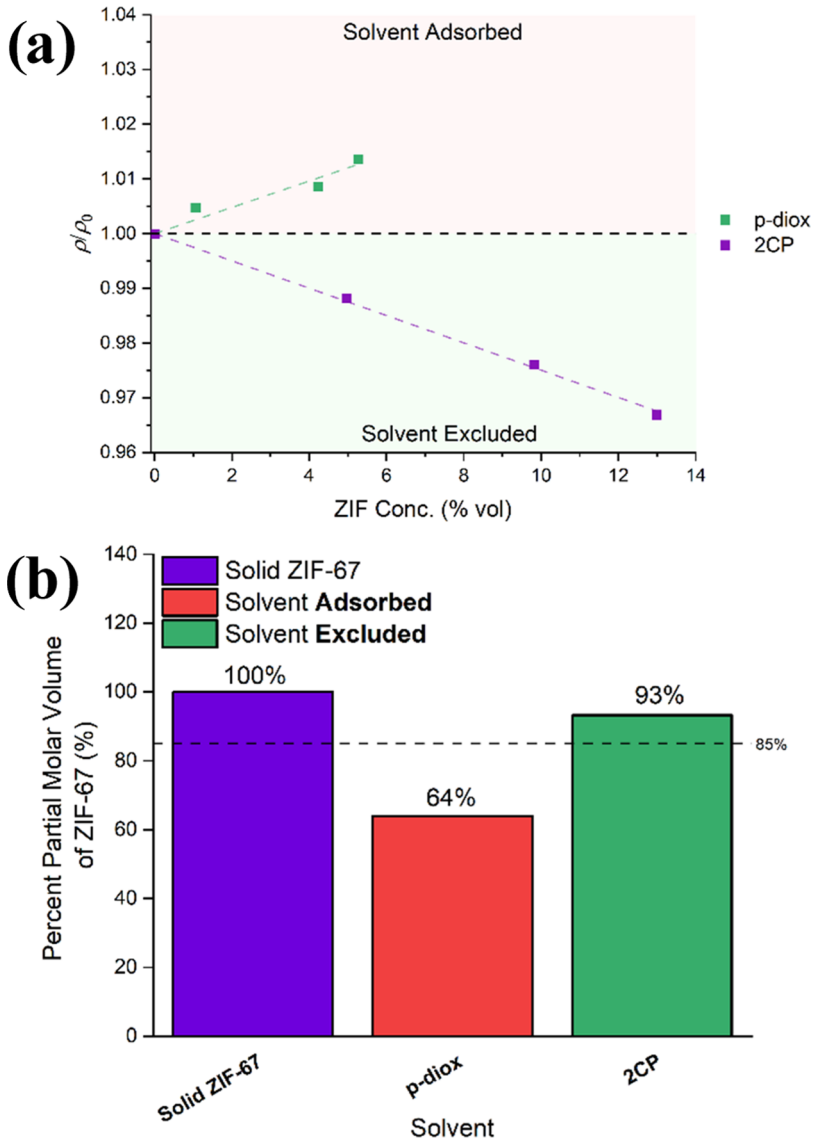

Figure 6. (a) Relative measured densities of dispersions at various weight loadings of ZIF−67 in p-dioxane (green squares) and 2CP (purple squares) and (b) the percent change in the partial molar volume of ZIF−67 in *p*-diox (red) and 2CP (green) compared to solid ZIF−67 (purple). The dashed line at 85% indicates the identified cutoff for PLs.

partial molar volume of ZIF−8. This is because the adsorption of these smaller solvent molecules decreases the volume contribution of ZIF−8 to the total volume of the dispersion.

3.6. Structure−Property Relationships Governing Solvent Exclusion in ZIF-Based PLs

Pore aperture expansion is expected to occur in all ZIF-based PLs; however, the effect that structural changes have on the aperture expansion is unknown. Again, utilizing the wide structural variety within the ZIF MOF family and experimental density measurements, the effects of metal percussor, pore aperture size, ligand functionality, and topology on aperture expansion and solvent exclusion in ZIF PLs were examined.

Both ZIF−67 and ZIF−71(SOD) are isostructural analogs of ZIF−8, differing from ZIF−8 in metal nodes (Co^{2+} versus Zn^{2+}) or ligands (4,5-dichloroimidazole versus 2-methylimidazole), respectively. Pore aperture expansion has been reported to occur to a lesser extent in ZIF−67 compared to ZIF−8;[39] but there are no experimental reports of the phenomenon occurring in ZIF−71(SOD). To examine this variable, density measurements of ZIF−67 dispersions in *p*-diox and 2CP solvents were performed and are shown in Figure 6a. Like ZIF−8, the density of ZIF−67 dispersions in *p*-diox increased with increasing ZIF−67 loading, while dispersions of ZIF−67 in 2CP decreased with increased ZIF loading. This indicates that replacing Zn^{2+} with Co^{2+} does not substantially affect the degree of pore aperture expansion or the size of solvent molecules excluded from the pores of the framework. Like ZIF−8, the partial molar volume of ZIF−67 dispersed in *p*-diox decreased almost 40%, Figure 6b. While the partial molar volume of ZIF−67 PL in 2CP changed less than 10%, further verification of PL formation occurred.

The bulky chloride functional groups of 4,5-dichloroimidazole lead to changes in the preferred ligand conformation within ZIF−71(SOD), causing an increase in the pore aperture size when compared to ZIF−8, Table S2. However, the effect these larger functionalities have on the expansion of the pore aperture and the steric exclusion of solvents is unknown. To examine this variable on ZIF−71(SOD), the density of ZIF dispersions in 2CP, 2HAP, DMI, and 15C5 solvents was

https://doi.org/10.1021/acsmaterialsau.3c00094
ACS Mater. Au 2024, 4, 224−237

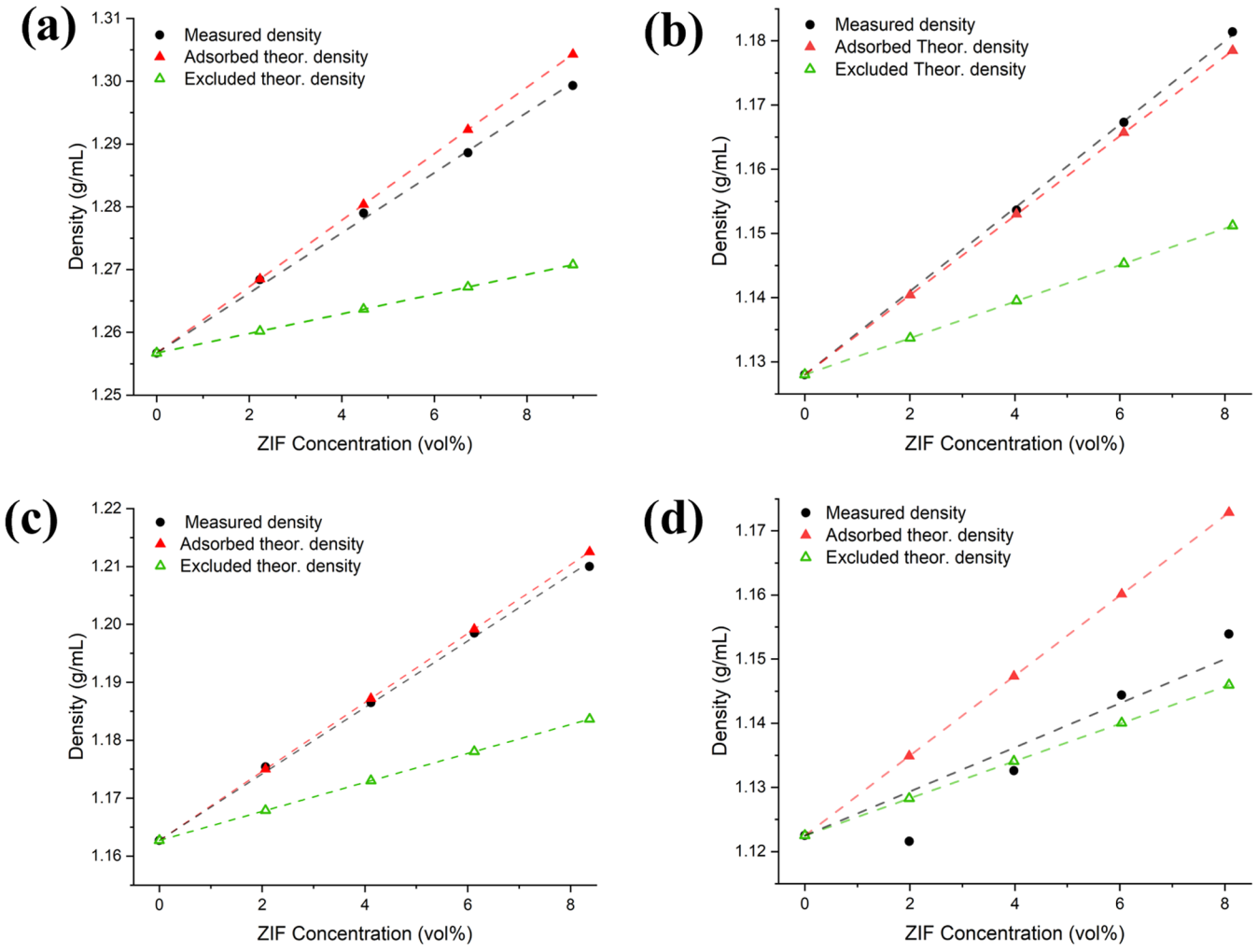

Figure 7. Comparison of measured (black circles) and theoretical densities (triangles), assuming solvent adsorbed (red triangles) or excluded (green triangles) of ZIF−71(SOD) dispersions in (a) 2CP, (b) 2HAP, (c) DMI, and (d) 15C5.

measured. These bulkier solvents were used to determine the range of excluded solvents due to the larger pores of ZIF−71(SOD). The structure, properties, and size of these solvents are provided in Tables S3 and S4. It should be noted, due to the larger crystallographic density of ZIF-71(SOD), that increased densities of dispersions are expected even when the solvent is excluded from the pores of the framework. Therefore, a comparison of measured densities with theoretical densities of the ZIF dispersions is required to confirm whether solvents are adsorbed or excluded from the pores.

Measured densities of ZIF−71(SOD) in 2CP, 2HAP, and DMI increased with increasing loading and aligned well with the adsorbed-theoretical densities, Figure 7a−c, which indicated that each solvent was adsorbed by the pores of ZIF−71(SOD). In comparison, the densities of ZIF−71(SOD) dispersions in 15C5 also increased with increasing ZIF loading, Figure 7d, but aligned with excluded-theoretical densities. This is further confirmed through comparison of the partial molar volumes of ZIF−71(SOD) in each solvent, Figure S24a. When dispersed in 15C5, the partial molar volume of ZIF−71(SOD) did not substantially change, while the partial molar volume of the ZIF in 2CP, 2HAP, and DMI all decreased by 20−40%. This made it evident that 15C5 was sterically too bulky and is excluded from the pores of the framework.

Additionally, these results illustrated that pore aperture expansion had occurred in ZIF−71(SOD) as solvents larger than the crystallographic pore aperture were adsorbed (2CP, 2HAP, and DMI). From these density measurements, it was determined that solvents with d_W > 6.9 Å/molecule possessed sufficient steric bulk to not be adsorbed by the pores of ZIF−71(SOD). This demonstrated that a 76% expansion of the pore aperture occurred to allow for the adsorption of the DMI solvent molecules. This degree of expansion is larger than the expansion observed in ZIF−8 (59%) dispersions, demonstrating that ligand functionality and ligand conformation within the framework positively impact the extent of pore aperture expansion within the ZIF frameworks.

Next, the pore aperture expansion in ZIFs possessing different topologies was examined by using ZIF−69 and ZIF−71(RHO), with GME and RHO topologies, respectively. An illustration of the structural differences between the three topologies is provided in Figure S8. The pore aperture and pore sizes of both ZIF−69 and ZIF−71(RHO) are the largest of the ZIFs examined, Table S2. Due to these larger pores, the bulky, and often more expensive, solvents 2HAP, DMI, and 15C5 were used to determine the range of excluded solvents.

The densities of ZIF−69 and −71(RHO) dispersed in each solvent at various ZIF loadings were measured. The densities of all ZIF-solvent dispersions increased with increasing ZIF

https://doi.org/10.1021/acsmaterialsau.3c00094
ACS Mater. Au 2024, 4, 224−237

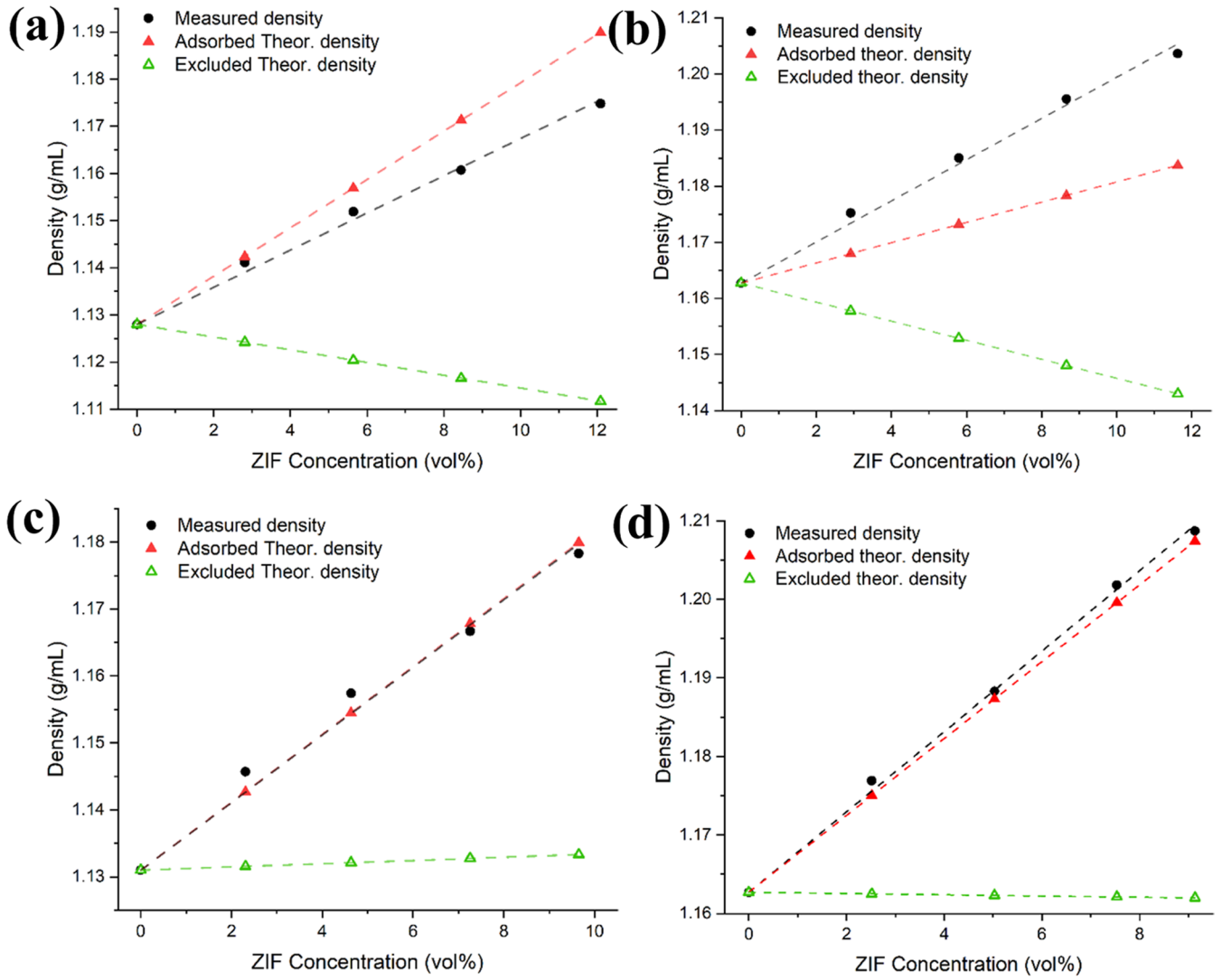

Figure 8. Comparison of measured (black circles) and theoretical densities (triangles), assuming solvent adsorbed (red triangles) or excluded (green triangles) of ZIF−69 (a, b) and ZIF−71(RHO) (c, d) dispersed at various loadings in 2HAP (a, c) and DMI (b, d).

loading, as illustrated in Figures 8 and 9. This contrasts with the expected densities, which decrease or stay relatively constant when the solvents are excluded from the pore space of ZIF−69 and ZIF−71(RHO), Table S2. When compared to theoretical densities the measured densities of ZIF−69 dispersion in 2HAP and DMI both match the adsorbed-theoretical densities, indicating that both solvents are adsorbed by ZIF−69. Though ZIF−71(RHO) possesses a smaller pore aperture than ZIF−69, the densities of ZIF−71(RHO) dispersions in 2HAP and DMI similarly matched the adsorbed-theoretical densities for both solvents. Again, this indicates that the large pore of ZIF−71(RHO) adsorbed the two solvents.

The adsorption of 2HAP and DMI by ZIF−69 and ZIF−71(RHO) indicated that pore aperture expansion also occurred in these ZIFs, allowing adsorption of the large solvent molecules. To further determine the limit of solvent molecule size for pore adsorption, solvent 15C5 was used. Figure 9 shows that the densities of both ZIF−69 and ZIF−71(RHO) increased with increasing ZIF loading. These measured densities of both ZIF−69 and ZIF−71(RHO) were lower than the solvent-adsorbed theoretically calculated densities. However, these results still indicate 15C5 adsorption by both ZIFs because the measured densities increased and were substantially larger than the solvent-excluded calculated densities, which decrease or remain almost constant with increasing ZIF loading. Furthermore, as shown in Figure S24b−c, the partial molar volumes of both ZIF−69 and ZIF−71(RHO) dispersed in 15C5 decreased by almost 20%. Compared with the partial molar volumes of PLs formed from ZIF−8, −67, and −71(SOD), all possessed decreases of less than 15% (see Figures S23 and S24a). Together this verified that 15C5 was adsorbed into the pores of both ZIF−67 and −71(RHO). Combining these results indicated that aperture expansion is occurring and the expansion of the apertures of both ZIF−69 and ZIF−71(RHO) is larger than 7.4 Å. This illustrates the limitations of ZIFs with larger pores to form Type 3 PLs with inexpensive and readily available solvents.

Comparing the extent of pore aperture expansion of all of the ZIFs, a design principle can be formulated. For ZIF−8 and −67, the pore aperture expanded more than 59%, while ZIF−71(SOD), with a larger pore aperture, possessed a greater degree of pore aperture expansion, increasing 76%. This

https://doi.org/10.1021/acsmaterialsau.3c00094
ACS Mater. Au 2024, 4, 224−237

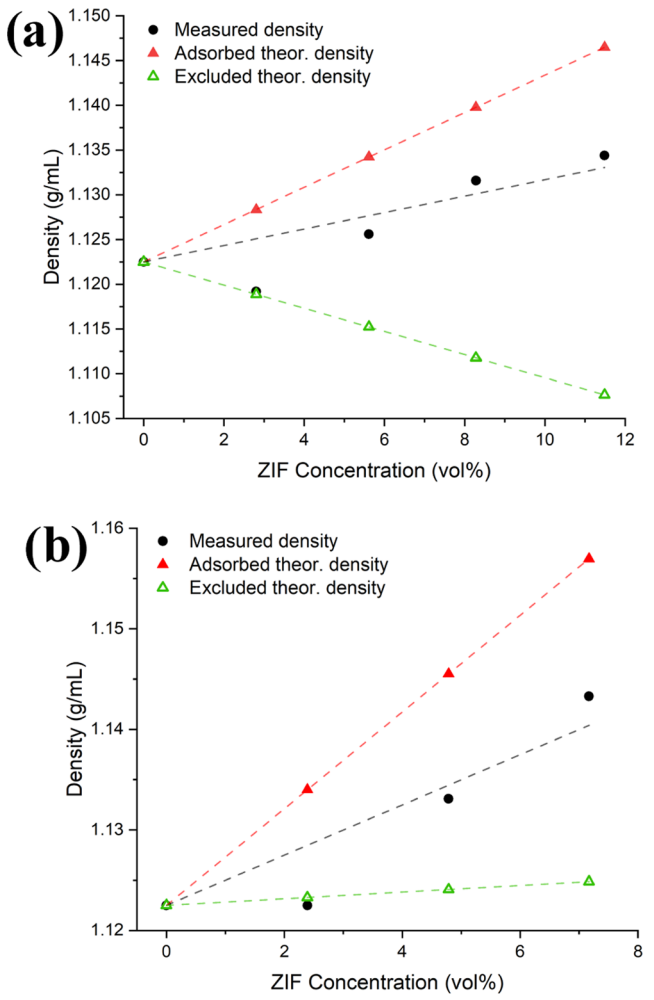

Figure 9. Comparison of measured (black circles) and theoretical densities (triangles), assuming solvent adsorbed (red triangles) or excluded (green triangles of a) ZIF−69 and (b) ZIF−71(RHO) dispersions in 15C5 at various weight loadings of ZIFs.

illustrated that the ligand conformation within the framework, determined by ligand functionality, impacts the degree of pore aperture expansion and the size of excluded solvents. ZIF−69 and ZIF−71(RHO), which possess different topologies, also showed substantial expansion of the pore apertures, 68 and 76%, respectively. Though the degree of expansion matches the other ZIFs examined, the limit of pore aperture expansion of these two ZIFs may be larger as no solvents larger than 15C5 were examined.

From these results, eight new ZIF-based Type 3 PLs were identified, five with organic solvents (ZIF−8 + 2CP, ZIF−8 + 2HAP, ZIF−8 + DHLC, ZIF−67 + 2CP, and ZIF−71(SOD) + 15C5) and three in water (ZIF−67 + water, ZIF−71(RHO) + water, and ZIF−71 (SOD) + water). Based on these new Type 3 PL systems, a material design principle was formed for developing new ZIF-based PLs, where solvents 1.8 times larger than the crystallographic pore aperture should be utilized to ensure steric exclusion from the pores. However, there are exceptions to this design principle. We also showed that the ligand functionality determined water exclusion from the ZIF pores, which illustrates the utility of ZIF/MOF tunability for Type 3 PLs, allowing for the nonsteric exclusion of solvents. This is critical for the formation of Type 3 PLs in aqueous solvent systems, especially for MOFs with large pore apertures.

4. CONCLUSIONS

Designing porous liquids for selective CO_2 gas capture requires exquisite control over the PL constituents (solvents and nanoporous host) to form a system tuned for CO_2 gas capture. Gaining a fundamental understanding of the permanent porosity of the MOF in the system is vital to enabling tuned gas adsorption locations. This has led to this focused study on the adsorption of individual solvents in ZIF MOFs in Type 3 PLs. Pore aperture expansion of ZIF−8 has been a barrier in predicting the ability to exclude solvent from within ZIF-8-based PL systems. Our computational calculations indicate that this aperture expansion allows for the adsorption of solvents commonly used in ZIF-based PLs. However, through simple density measurements, we elucidated the impacts and limits of aperture expansion on the adsorption solvents in a series ZIF-based PLs. From these results, eight new ZIF-based Type 3 PLs were discovered. We further illustrated the use of partial molar volumes for the facile verification of Type 3 PLs, even when formed from different porous hosts or solvents. We propose that to effectively make ZIF-based PLs with accessible pores for gas adsorption, solvents with molecular sizes 1.8 times or larger than the crystallographic pore aperture of the ZIF should be used. Furthermore, our computational calculations suggest the importance of the pore aperture in gas−PL interactions allowing for additional tuning sites to improve the gas capture capabilities of Type 3 PLs.

■ ASSOCIATED CONTENT

Supporting Information

The Supporting Information is available free of charge at https://pubs.acs.org/doi/10.1021/acsmaterialsau.3c00094.

Comparison of the properties of solvents and ZIFs, N_2 gas adsorption of ZIFs, images taken from computational calculations, additional XRD and FTIR data of all dispersions, additional density measurement plots dispersions, TGA-MS plots of mixed solvent dispersions of ZIF−8 aqueous dispersion of ZIF−71(RHO), and coordinates of the molecular simulations (PDF)

output_POSCARs (ZIP)

■ AUTHOR INFORMATION

Corresponding Author

Tina M. Nenoff − *Advanced Science and Technology, Sandia National Laboratories, Albuquerque, New Mexico 87185, United States;* orcid.org/0000-0002-7906-4810; Email: tmnenof@sandia.gov

Authors

Matthew J. Hurlock − *Nanoscale Sciences Department, Sandia National Laboratories, Albuquerque, New Mexico 87185, United States;* orcid.org/0000-0002-0262-2095

Matthew S. Christian − *Geochemistry Department, Sandia National Laboratories, Albuquerque, New Mexico 87185, United States;* orcid.org/0000-0002-3416-413X

Jessica M. Rimsza − *Geochemistry Department, Sandia National Laboratories, Albuquerque, New Mexico 87185, United States;* orcid.org/0000-0003-0492-852X

Complete contact information is available at: https://pubs.acs.org/10.1021/acsmaterialsau.3c00094

https://doi.org/10.1021/acsmaterialsau.3c00094
ACS Mater. Au 2024, 4, 224−237

Author Contributions

M.J.H.: data curation, experimental analysis, investigation, methodology, writing—original draft, writing—review and editing, M.S.C.: data curation, formal analysis, writing—review and editing; J.M.R.: conceptualization, writing—reviewing and editing; T.M.N.: conceptualization, project administration, resources, writing—review and editing.

Funding

The work described here was supported as part of the Center for Understanding and Controlling Accelerated and Gradual Evolution of Materials for Energy (UNCAGE-ME), an Energy Frontier Research Center funded by the U.S. Department of Energy, Office of Science, Basic Energy Sciences under Award #DE-SC0012577.

Notes

The authors declare no competing financial interest.

■ ACKNOWLEDGMENTS

This article has been authored by an employee of National Technology & Engineering Solutions of Sandia, LLC under Contract No. DE-NA0003525 with the U.S. Department of Energy (DOE). The employee owns all right, title, and interest in and to the article and is solely responsible for its contents. The U.S. Government and the publisher, by accepting the article for publication, acknowledge that the U.S. Government retains a nonexclusive, paid-up, irrevocable, worldwide license to publish or reproduce the published form of this article or allow others to do so, for U.S. Government purposes. The DOE will provide public access to all results of federally sponsored research in accordance with the DOE Public Access Plan: https://www.energy.gov/downloads/doe-public-access-plan.

■ REFERENCES

(1) O'Reilly, N.; Giri, N.; James, S. L. Porous Liquids. *Chem. - Eur. J.* **2007**, *13* (11), 3020−3025.
(2) Rimsza, J. M.; Nenoff, T. M. Porous Liquids: Computational Design for Targeted Gas Adsorption. *ACS Appl. Mater. Interfaces* **2022**, *14* (16), 18005−18015.
(3) Wang, D.; Xin, Y.; Yao, D.; Li, X.; Ning, H.; Zhang, H.; Wang, Y.; Ju, X.; He, Z.; Yang, Z.; Fan, W.; Li, P.; Zheng, Y. Shining Light on Porous Liquids: From Fundamentals to Syntheses, Applications and Future Challenges. *Adv. Funct. Mater.* **2022**, *32* (1), No. 2104162.
(4) Mahdavi, H.; Smith, S. J. D.; Mulet, X.; Hill, M. R. Practical considerations in the design and use of porous liquids. *Mater. Horiz.* **2022**, *9* (6), 1577−1601.
(5) Li, Y. Research Progress of Porous Liquids. *ChemistrySelect* **2020**, *5* (43), 13664−13672.
(6) Li, H.; Chen, W.; Liu, B.; Jia, C.; Qiao, Z.; Sun, C.; Yang, L.; Ma, Q.; Chen, G. CO2 capture using ZIF-8/water-glycol-2-methylimidazole slurry with high capacity and low desorption heat. *Chem. Eng. Sci.* **2018**, *182*, 189−199.
(7) Shi, T.; Zheng, Y.; Wang, T.; Li, P.; Wang, Y.; Yao, D. Effect of Pore Size on the Carbon Dioxide Adsorption Behavior of Porous Liquids Based on Hollow Silica. *ChemPhysChem* **2018**, *19* (1), 130−137.
(8) Wang, D.; Xin, Y.; Li, X.; Wang, F.; Wang, Y.; Zhang, W.; Zheng, Y.; Yao, D.; Yang, Z.; Lei, X. A universal approach to turn UiO-66 into type 1 porous liquids via post-synthetic modification with corona-canopy species for CO2 capture. *J. Chem. Eng.* **2021**, *416*, No. 127625.
(9) Sheng, L.; Chen, Z.; Wang, X.; Farooq, A. S. Transforming Porous Silica Nanoparticles into Porous Liquids with Different Canopy Structures for CO2 Capture. *ACS Omega* **2022**, *7* (7), 5687−5697.
(10) Giri, N.; Del Pópolo, M. G.; Melaugh, G.; Greenaway, R. L.; Rätzke, K.; Koschine, T.; Pison, L.; Gomes, M. F. C.; Cooper, A. I.; James, S. L. Liquids with permanent porosity. *Nature* **2015**, *527* (7577), 216−220.
(11) Egleston, B. D.; Luzyanin, K. V.; Brand, M. C.; Clowes, R.; Briggs, M. E.; Greenaway, R. L.; Cooper, A. I. Controlling Gas Selectivity in Molecular Porous Liquids by Tuning the Cage Window Size. *Angew. Chem., Int. Ed.* **2020**, *59* (19), 7362−7366.
(12) Rimsza, J.; Nenoff, T. M. Design of enhanced porous organic cage solubility in Type 2 porous liquids. *J. Mol. Liq.* **2023**, *377*, No. 121536, DOI: 10.1016/j.molliq.2023.121536.
(13) Shan, W.; Fulvio, P. F.; Kong, L.; Schott, J. A.; Do-Thanh, C.-L.; Tian, T.; Hu, X.; Mahurin, S. M.; Xing, H.; Dai, S. New Class of Type III Porous Liquids: A Promising Platform for Rational Adjustment of Gas Sorption Behavior. *ACS Appl. Mater. Interfaces* **2018**, *10* (1), 32−36, DOI: 10.1021/acsami.7b15873.
(14) Cahir, J.; Tsang, M. Y.; Lai, B.; Hughes, D.; Alam, M. A.; Jacquemin, J.; Rooney, D.; James, S. L. Type 3 porous liquids based on non-ionic liquid phases − a broad and tailorable platform of selective, fluid gas sorbents. *Chem. Sci.* **2020**, *11* (8), 2077−2084.
(15) Brand, M. C.; Rankin, N.; Cooper, A. I.; Greenaway, R. L. Photoresponsive Type III Porous Liquids. *Chem. - Eur. J.* **2023**, *29* (4), No. e202202848.
(16) Kai, A.; Egleston, B. D.; Tarzia, A.; Clowes, R.; Briggs, M. E.; Jelfs, K. E.; Cooper, A. I.; Greenaway, R. L. Modular Type III Porous Liquids Based on Porous Organic Cage Microparticles. *Adv. Funct. Mater.* **2021**, *31* (51), No. 2106116.
(17) Gaillac, R.; Pullumbi, P.; Beyer, K. A.; Chapman, K. W.; Keen, D. A.; Bennett, T. D.; Coudert, F.-X. Liquid metal−organic frameworks. *Nat. Mater.* **2017**, *16* (11), 1149−1154.
(18) Pardakhti, M.; Jafari, T.; Tobin, Z.; Dutta, B.; Moharreri, E.; Shemshaki, N. S.; Suib, S.; Srivastava, R. Trends in Solid Adsorbent Materials Development for CO2 Capture. *ACS Appl. Mater. Interfaces* **2019**, *11* (38), 34533−34559.
(19) Wang, C.; Liu, D.; Lin, W. Metal−Organic Frameworks as A Tunable Platform for Designing Functional Molecular Materials. *J. Am. Chem. Soc.* **2013**, *135* (36), 13222−13234.
(20) Abraha, Y. W.; Tsai, C.-W.; Niemantsverdriet, J. W. H.; Langner, E. H. G. Optimized CO2 Capture of the Zeolitic Imidazolate Framework ZIF-8 Modified by Solvent-Assisted Ligand Exchange. *ACS Omega* **2021**, *6* (34), 21850−21860.
(21) Lin, R.-B.; Xiang, S.; Zhou, W.; Chen, B. Microporous Metal-Organic Framework Materials for Gas Separation. *Chem* **2020**, *6* (2), 337−363.
(22) Zhang, W.; Taheri-Ledari, R.; Saeidirad, M.; Qazi, F. S.; Kashtiaray, A.; Ganjali, F.; Tian, Y.; Maleki, A. Regulation of Porosity in MOFs: A Review on Tunable Scaffolds and Related Effects and Advances in Different Applications. *J. Environ. Chem. Eng.* **2022**, *10* (6), No. 108836.
(23) Kazemi, S.; Safarifard, V. Carbon dioxide capture in MOFs: The effect of ligand functionalization. *Polyhedron* **2018**, *154*, 236−251.
(24) Knebel, A.; Bavykina, A.; Datta, S. J.; Sundermann, L.; Garzon-Tovar, L.; Lebedev, Y.; Durini, S.; Ahmad, R.; Kozlov, S. M.; Shterk, G.; Karunakaran, M.; Carja, I. D.; Simic, D.; Weilert, I.; Klüppel, M.; Giese, U.; Cavallo, L.; Rueping, M.; Eddaoudi, M.; Caro, J.; Gascon, J. Solution processable metal−organic frameworks for mixed matrix membranes using porous liquids. *Nat. Mater.* **2020**, *19* (12), 1346−1353.
(25) Wang, D.; Xin, Y.; Li, X.; Ning, H.; Wang, Y.; Yao, D.; Zheng, Y.; Meng, Z.; Yang, Z.; Pan, Y.; Li, P.; Wang, H.; He, Z.; Fan, W. Transforming Metal−Organic Frameworks into Porous Liquids via a Covalent Linkage Strategy for CO2 Capture. *ACS Appl. Mater. Interfaces* **2021**, *13* (2), 2600−2609.
(26) Qi, Z.; Qiu, T.; Wang, H.; Ye, C. Synthesis of ionic-liquid-functionalized UiO-66 framework by post-synthetic ligand exchange for the ultra-deep desulfurization. *Fuel* **2020**, *268*, No. 117336.

(27) Liu, S.; Liu, J.; Hou, X.; Xu, T.; Tong, J.; Zhang, J.; Ye, B.; Liu, B. Porous Liquid: A Stable ZIF-8 Colloid in Ionic Liquid with Permanent Porosity. *Langmuir* **2018**, *34* (12), 3654−3660.
(28) Liu, H.; Liu, B.; Lin, L.-C.; Chen, G.; Wu, Y.; Wang, J.; Gao, X.; Lv, Y.; Pan, Y.; Zhang, X.; Zhang, X.; Yang, L.; Sun, C.; Smit, B.; Wang, W. A hybrid absorption−adsorption method to efficiently capture carbon. *Nat. Commun.* **2014**, *5* (1), No. 5147.
(29) Wu, J.; Wu, X.; Zhao, P.; Wang, Z.; Zhang, L.; Xu, D.; Gao, J. Extraction desulphurization of fuels using ZIF-8-based porous liquid. *Fuel* **2021**, *300*, No. 121013.
(30) Mahdavi, H.; Zhang, H.; Macreadie, L. K.; Doherty, C. M.; Acharya, D.; Smith, S. J. D.; Mulet, X.; Hill, M. R. Underlying solvent-based factors that influence permanent porosity in porous liquids. *Nano Res.* **2022**, *15* (4), 3533−3538.
(31) Erdosy, D. P.; Wenny, M. B.; Cho, J.; DelRe, C.; Walter, M. V.; Jiménez-Ángeles, F.; Qiao, B.; Sanchez, R.; Peng, Y.; Polizzotti, B. D.; de la Cruz, M. O.; Mason, J. A. Microporous water with high gas solubilities. *Nature* **2022**, *608* (7924), 712−718.
(32) Liu, H.; Yao, D.; Li, H.; Li, R.; Wang, J. The experimental and theory research on the sorption kinetic of CH4 and C2H4 in ZIF-8/water-glycol slurry. *Microporous Mesoporous Mater.* **2022**, *329*, No. 111559.
(33) Yang, M.; Wang, H.; Zuo, J. Y.; Deng, C.; Liu, B.; Chai, L.; Li, K.; Xiao, H.; Xiao, P.; Wang, X.; Chen, W.; Peng, X.; Han, Y.; Huang, Z.; Dong, B.; Sun, C.; Chen, G. Efficient separation of butane isomers via ZIF-8 slurry on laboratory- and pilot-scale. *Nat. Commun.* **2022**, *13* (1), No. 4792.
(34) Hurlock, M. J.; Christian, M. S.; Fritzsching, K. J.; Rademacher, D. X.; Rimsza, J. M.; Nenoff, T. M. Experimental and Computational Mechanisms that Govern Long-Term Stability of CO2-Adsorbed ZIF-8-Based Porous Liquids. *ACS Appl. Mater. Interfaces* **2023**, *15* (27), 32792−32802.
(35) Zhang, K.; Lively, R. P.; Zhang, C.; Chance, R. R.; Koros, W. J.; Sholl, D. S.; Nair, S. Exploring the Framework Hydrophobicity and Flexibility of ZIF-8: From Biofuel Recovery to Hydrocarbon Separations. *J. Phys. Chem. Lett.* **2013**, *4* (21), 3618−3622.
(36) Fairen-Jimenez, D.; Moggach, S. A.; Wharmby, M. T.; Wright, P. A.; Parsons, S.; Düren, T. Opening the Gate: Framework Flexibility in ZIF-8 Explored by Experiments and Simulations. *J. Am. Chem. Soc.* **2011**, *133* (23), 8900−8902.
(37) Casco, M. E.; Cheng, Y. Q.; Daemen, L. L.; Fairen-Jimenez, D.; Ramos-Fernández, E. V.; Ramirez-Cuesta, A. J.; Silvestre-Albero, J. Gate-opening effect in ZIF-8: the first experimental proof using inelastic neutron scattering. *Chem. Commun.* **2016**, *52* (18), 3639−3642.
(38) Boada, R.; Chaboy, J.; Hayama, S.; Keenan, L. L.; Freeman, A. A.; Amboage, M.; Díaz-Moreno, S. Unraveling the Molecular Details of the "Gate Opening" Phenomenon in ZIF-8 with X-ray Absorption Spectroscopy. *J. Phys. Chem. C* **2022**, *126* (13), 5935−5943.
(39) Mor, J.; Utpalla, P.; Mukherjee, S.; Sharma, S. K.; Dutta, D. Gate Opening Induced High Pore Volume Expansion in Flexible Zeolitic Imidazole Frameworks during CO2 Adsorption: A Direct Observation Using Positron Annihilation Spectroscopy. *J. Phys. Chem. C* **2023**, *127* (5), 2160−2172.
(40) Vogel, D. J.; Nenoff, T. M.; Rimsza, J. M. Design Elements for Enhanced Hydrogen Isotope Separations in Barely Porous Organic Cages. *ACS Omega* **2022**, *7* (9), 7963−7972.
(41) Thomas, A.; Prakash, M. The Role of Binary Mixtures of Ionic Liquids in ZIF-8 for Selective Gas Storage and Separation: A Perspective from Computational Approaches. *J. Phys. Chem. C* **2020**, *124* (48), 26203−26213.
(42) Thomas, A.; Kamalakannan, S.; Cheriyan, A.; Prakash, M. Theoretical studies on the role of water in ionic liquids at ZIF (IL@ZIF) complex and its effect on selective CO2 separation. *Mater. Today Sustainability* **2023**, *22*, No. 100376.
(43) Fairen-Jimenez, D.; Galvelis, R.; Torrisi, A.; Gellan, A. D.; Wharmby, M. T.; Wright, P. A.; Mellot-Draznieks, C.; Düren, T. Flexibility and swing effect on the adsorption of energy-related gases on ZIF-8: combined experimental and simulation study. *Dalton Trans.* **2012**, *41* (35), 10752−10762.
(44) Verploegh, R. J.; Nair, S.; Sholl, D. S. Temperature and Loading-Dependent Diffusion of Light Hydrocarbons in ZIF-8 as Predicted Through Fully Flexible Molecular Simulations. *J. Am. Chem. Soc.* **2015**, *137* (50), 15760−15771.
(45) Li, D.; Zhang, P.; Kang, Q.; Han, Y.; Shen, D. Investigation of the effect of energy variation and structure change on the adsorption of volatile organic compounds in ZIF-8 by a DFT approach. *Microporous Mesoporous Mater.* **2017**, *248*, 84−90.
(46) Hobday, C. L.; Woodall, C. H.; Lennox, M. J.; Frost, M.; Kamenev, K.; Düren, T.; Morrison, C. A.; Moggach, S. A. Understanding the adsorption process in ZIF-8 using high pressure crystallography and computational modelling. *Nat. Commun.* **2018**, *9* (1), No. 1429.
(47) Thomas, A.; Maiyelvaganan, K. R.; Kamalakannan, S.; Prakash, M. Density Functional Theory Studies on Zeolitic Imidazolate Framework-8 and Ionic Liquid-Based Composite Materials. *ACS Omega* **2019**, *4* (27), 22655−22666.
(48) Fan, T.; Chen, L.; Qiu, S.; Yang, C.; Hu, L.; Peng, X.; Zhang, J.; Yan, Z. Synthesis of hierarchical porous ZIF-8/3DCNTs composite sensor for ultrasensitive detection of DA and DFT studies. *J. Electroanal. Chem.* **2020**, *878*, No. 114541.
(49) Lewis, D. W.; Ruiz-Salvador, A. R.; Gómez, A.; Rodriguez-Albelo, L. M.; Coudert, F.-X.; Slater, B.; Cheetham, A. K.; Mellot-Draznieks, C. Zeolitic imidazole frameworks: structural and energetics trends compared with their zeolite analogues. *CrystEngComm* **2009**, *11* (11), 2272−2276.
(50) Blum, V.; Gehrke, R.; Hanke, F.; Havu, P.; Havu, V.; Ren, X.; Reuter, K.; Scheffler, M. Ab initio molecular simulations with numeric atom-centered orbitals. *Comput. Phys. Commun.* **2009**, *180* (11), 2175−2196.
(51) Havu, V.; Blum, V.; Havu, P.; Scheffler, M. Efficient O(N) integration for all-electron electronic structure calculation using numeric basis functions. *J. Comput. Phys.* **2009**, *228* (22), 8367−8379.
(52) Marek, A.; Blum, V.; Johanni, R.; Havu, V.; Lang, B.; Auckenthaler, T.; Heinecke, A.; Bungartz, H. J.; Lederer, H. The ELPA library: scalable parallel eigenvalue solutions for electronic structure theory and computational science. *J. Phys.: Condens. Matter* **2014**, *26* (21), No. 213201, DOI: 10.1088/0953-8984/26/21/213201.
(53) Ren, X.; Rinke, P.; Blum, V.; Wieferink, J.; Tkatchenko, A.; Sanfilippo, A.; Reuter, K.; Scheffler, M. Resolution-of-identity approach to Hartree−Fock, hybrid density functionals, RPA, MP2 and GW with numeric atom-centered orbital basis functions. *New J. Phys.* **2012**, *14* (5), No. 053020.
(54) Tkatchenko, A.; Scheffler, M. Accurate Molecular Van Der Waals Interactions from Ground-State Electron Density and Free-Atom Reference Data. *Phys. Rev. Lett.* **2009**, *102* (7), No. 073005.
(55) Bhattacharyya, S.; Han, R.; Kim, W.-G.; Chiang, Y.; Jayachandrababu, K. C.; Hungerford, J. T.; Dutzer, M. R.; Ma, C.; Walton, K. S.; Sholl, D. S.; Nair, S. Acid Gas Stability of Zeolitic Imidazolate Frameworks: Generalized Kinetic and Thermodynamic Characteristics. *Chem. Mater.* **2018**, *30* (12), 4089−4101.
(56) Borne, I.; Saigal, K.; Jones, C. W.; Lively, R. P. Thermodynamic Evidence for Type II Porous Liquids. *Ind. Eng. Chem. Res.* **2023**, *62* (29), 11689−11696.
(57) Banerjee, R.; Phan, A.; Wang, B.; Knobler, C.; Furukawa, H.; O'Keeffe, M.; Yaghi, O. M. High-Throughput Synthesis of Zeolitic Imidazolate Frameworks and Application to CO2 Capture. *Science* **2008**, *319* (5865), 939−943.
(58) Kwon, H. T.; Jeong, H.-K.; Lee, A. S.; An, H. S.; Lee, J. S. Heteroepitaxially Grown Zeolitic Imidazolate Framework Membranes with Unprecedented Propylene/Propane Separation Performances. *J. Am. Chem. Soc.* **2015**, *137* (38), 12304−12311.
(59) Hafizovic, J.; Bjørgen, M.; Olsbye, U.; Dietzel, P. D. C.; Bordiga, S.; Prestipino, C.; Lamberti, C.; Lillerud, K. P. The Inconsistency in Adsorption Properties and Powder XRD Data of MOF-5 Is Rationalized by Framework Interpenetration and the

Presence of Organic and Inorganic Species in the Nanocavities. *J. Am. Chem. Soc.* **2007**, *129* (12), 3612−3620.
(60) Yakovenko, A. A.; Wei, Z.; Wriedt, M.; Li, J.-R.; Halder, G. J.; Zhou, H.-C. Study of Guest Molecules in Metal−Organic Frameworks by Powder X-ray Diffraction: Analysis of Difference Envelope Density. *Cryst. Growth Des.* **2014**, *14* (11), 5397−5407.
(61) Schweinefuß, M. E.; Springer, S.; Baburin, I. A.; Hikov, T.; Huber, K.; Leoni, S.; Wiebcke, M. Zeolitic imidazolate framework-71 nanocrystals and a novel SOD-type polymorph: solution mediated phase transformations, phase selection via coordination modulation and a density functional theory derived energy landscape. *Dalton Trans.* **2014**, *43* (9), 3528−3536.
(62) Springer, S.; Baburin, I. A.; Heinemeyer, T.; Schiffmann, J. G.; van Wüllen, L.; Leoni, S.; Wiebcke, M. A zeolitic imidazolate framework with conformational variety: conformational polymorphs versus frameworks with static conformational disorder. *CrystEngComm* **2016**, *18* (14), 2477−2489.
(63) Ortiz, A. U.; Freitas, A. P.; Boutin, A.; Fuchs, A. H.; Coudert, F.-X. What makes zeolitic imidazolate frameworks hydrophobic or hydrophilic? The impact of geometry and functionalization on water adsorption. *Phys. Chem. Chem. Phys.* **2014**, *16* (21), 9940−9949.
(64) Knight, A. W.; Kalugin, N. G.; Coker, E.; Ilgen, A. G. Water properties under nano-scale confinement. *Sci. Rep.* **2019**, *9* (1), No. 8246.
(65) Zhang, K.; Lively, R. P.; Dose, M. E.; Brown, A. J.; Zhang, C.; Chung, J.; Nair, S.; Koros, W. J.; Chance, R. R. Alcohol and water adsorption in zeolitic imidazolate frameworks. *Chem. Commun.* **2013**, *49* (31), 3245−3247.
(66) Lively, R. P.; Dose, M. E.; Thompson, J. A.; McCool, B. A.; Chance, R. R.; Koros, W. J. Ethanol and water adsorption in methanol-derived ZIF-71. *Chem. Commun.* **2011**, *47* (30), 8667−8669.
(67) Zhao, Y. H.; Abraham, M. H.; Zissimos, A. M. Fast Calculation of van der Waals Volume as a Sum of Atomic and Bond Contributions and Its Application to Drug Compounds. *J. Org. Chem.* **2003**, *68* (19), 7368−7373.

https://doi.org/10.1021/acsmaterialsau.3c00094
ACS Mater. Au 2024, 4, 224−237